

Anyonic Braiding in a Chiral Mach-Zehnder Interferometer

Bikash Ghosh^{*,1}, Maria Labendik^{*,1}, Liliia Musina¹, Vladimir Umansky¹,
Moty Heiblum^{1,#}, and David F. Mross²

¹ Braun Center for Submicron Research & Department of Condensed Matter Physics

² Department of Condensed Matter Physics

Weizmann Institute of Science, Rehovot, Israel

* Equal contributions

Corresponding author

Fractional quantum statistics are a signature prediction of fractional quantum Hall states, which have long been elusive in experiments. Here, we present the observation of anyonic interference and exchange phases in a novel *co-propagating* 'optical-like' Mach-Zehnder Interferometer. This architecture is free of charging and backscattering effects that often plague the widely used Fabry-Perot interferometer, thus exhibiting pristine Aharonov-Bohm (AB) interference without fractional phase slips. We studied the three lowest Jain filling factors, $\nu = 1/3, 2/5,$ and $3/7,$ which host quasiparticles with fractional charges $e^* = e/3, e/5,$ and $e/7,$ respectively. The observed AB interference patterns, plotted as a function of magnetic field B and modulation-gate voltage, V_{MG} (known as *pajamas*), exhibited the expected flux periodicities: $3\Phi_0, 5\Phi_0,$ and $7\Phi_0,$ with Φ_0 being the flux quantum. A small biased top gate (TG) deposited in the center of the interferometer induces local quasiparticles that are spatially isolated from the interfering modes. At non-zero TG voltage $V_{\text{TG}},$ quantized *phase slips* appear in the AB pajamas approximately with every flux quantum that pierces the effective area below the TG. Moreover, when tuning $V_{\text{TG}},$ at a constant magnetic field, abrupt phase jumps corresponding to adding one localized quasiparticle at a time under the top gate appear in the $B-V_{\text{TG}}$ pajamas.

Quantum Hall states are quintessential examples of topological phases of matter ([1](#)). In particular, the fractional states host quasiparticle (QP) excitations that carry fractional charges ([2-4](#)) and

exhibit *anyonic* statistics (5-8). Upon exchanging two identical QPs, the phase of their joint wavefunction changes by a fraction of π , unlike the behavior of fermions (bosons), where the exchange phase is π (2π) (9). Two key methods for probing these anyonic statistics involve interference in space (10) or time (11, 12). In the spatial domain, the phase difference between two quasiparticle trajectories consists of an Aharonov-Bohm (AB) phase, which depends on the enclosed flux and a statistical phase determined by the number of the enclosed QPs. For bosons or fermions, the statistical phase is an unobservable multiple of 2π , but it becomes measurable in systems hosting anyons (13, 14). QPs can either be localized in the bulk (with a significant excitation energy) or delocalized in chiral edge modes at the periphery of the bulk (with a smaller excitation energy).

Interference studies with fractional quantum Hall (FQH) states utilize two primary architectures: the Fabry-Perot Interferometer (FPI) (10, 15-19) and the Mach-Zehnder Interferometer (MZI) (20-22). In the FPI, a quantum Hall bulk is bounded from two sides by regions of a lower filling factor (Figure 1c). The interference loop consists of counter-propagating charge modes on opposite sides of the central area. The loop is partially closed by two quantum point contacts (QPCs) that only allow tunneling of specific charges whose quantization is set by the bulk filling. Figure 1c illustrates the essential features of the FPI for the integer case using semiclassical electron trajectories. In particular, closed paths within the central region correspond to localized quasiparticles within the interference loop. Promoting electrons to composite fermions (CFs) results in the fractional regime where the excitation of localized QPs changes the phase of the interfering QPs in discrete steps, i.e., they cause phase slips. In reality, the transmission through the FPI is additionally influenced by a 'breathing' of the AB area with the magnetic field and, most importantly, by intrinsic charging energy for adding QPs to its central region (23-27). Still, sufficient screening of the Coulomb interaction allowed observation of phase slips, which approximately agree with the expected braiding phases (26-29).

The conventional MZI, by contrast, contains an internal grounded drain, which renders it free of charging effects. However, this drain also makes it subject to the Byers-Yang argument (30), which predicts $1\Phi_0$ periodicity (31). Physically, this periodicity arises because QPs returning to the internal loop continuously 'dress' the AB interference of fractional charges by their braiding

phase (32-34). Phase slips were neither observed (34) nor expected in the MZI (32); however, the visibility profile (as a function of the MZI transmission) is drastically different from that in the integer regime, consistent with its origin in anyonic interference (34).

An Optical-like Mach-Zehnder Interferometer (OMZI) combines the MZI's immunity to charging effects with the FPI's ability to observe significant AB periodicities and anyonic braiding. It was first constructed and tested by Deviatov *et al.* in 2012 (35) but without conclusive results. A theoretical study by Batra *et al.* (36) presented an exact solution for specific edge modes (36). The OMZI structure is drawn schematically in Figure 1a. It comprises three regions, each with a different filling factor. The central (bulk) region is tuned to filling ν_b while being bounded by two regions that are gate-tuned to an *upper* filling, $\nu_u > \nu_b$, and to a *lower* filling $\nu_l < \nu_b$ - leading to two *co-propagating* interface charged modes with corresponding 'fillings': $\nu_u - \nu_b$ and $\nu_b - \nu_l$ (37). Current emanating from source S1 (or source S2) is partitioned by the input QPC1 to two forward-propagating chiral interface modes. After surrounding the bulk, the two interface modes are re-partitioned by the output QPC2, and the current is eventually collected by drain D1 (or drain D2). Chirality of the charge modes ensures that all the sourced current passes through the OMZI and is not subject to charging effects. Additionally, the potential landscape, which exhibits a saddle instead of a valley in the central region, implies the absence of localized low-energy QPs inside the interference loop (Figure 1c). These two features distinguish the OMZI from the FPI, leading the OMZI to support pristine AB interference without phase slips.

To observe anyonic braiding, the QPs must be introduced into the OMZI by a separate mechanism. For this purpose, we employ a top gate (TG) that locally depletes (partially) the charge upon application of a negative gate voltage. The reduced filling factor under the gate leads to an edge mode in its periphery, which supports fractionally quantized charged excitations (encoded as the winding number of the edge mode). These QPs have lower energies than bulk quasiparticles and can be pushed across the Fermi level by varying the gate voltage or the magnetic field. Thereupon, fractional charge transfers from the gapless outer boundary of the OMZI to the inner edge mode encircling the top gated region. The resulting QPs in the center of

the OMZI are spatially isolated from the interfering QPs and affect them *solely* via statistical phases.

Our OMZI (Figures 1a & 1b) is fabricated in a 2DEG, induced in GaAs-AlGaAs heterostructure, with a density of $1.07 \times 10^{11} \text{cm}^{-2}$ and ‘dark mobility’ $4.5 \times 10^6 \text{cm}^2/\text{V-S}$ at 4.2K. Measurements are performed at the electrons’ temperature of $\sim 15 \text{mK}$. The fabricated internal area of the OMZI is $A = 3 \mu\text{m}^2$, with a single path length of $3 \mu\text{m}$. Due to the gates’ depletion, the actual OMZI area is $A \cong 2.9 \mu\text{m}^2$, though its internal area is also affected by the pinching voltage of the QPCs. An additional small ‘top gate’ (TG) with an area $A_{\text{TG}} = 0.785 \mu\text{m}^2$ is deposited in the center of the interferometer’s bulk, biased via an *air bridge* (Figure 1b). A small AC signal ($\sim 2 \mu\text{V}_{\text{RMS}}$), at a frequency of 776kHz, is applied to S1. The interfering signal reaches D1 and is filtered by an LC circuit (tuned to the input frequency with a BW=30kHz). The signal is subsequently amplified by a cooled amplifier to 4.2K (Gain=10), followed by a room-temperature amplifier (Gain=400). A spectrum analyzer, tuned to the carrier frequency, with a narrow bandwidth BW=5Hz, measures the amplified output signal.

We tested three configurations, each with a different fractional bulk filling, i.e., $\nu_b = 1/3$, $\nu_b = 2/5$, and $\nu_b = 3/7$. The upper and lower gated regions were chosen to realize two co-propagating interface modes formed in the following configurations: $\nu_u - \nu_b - \nu_l = 2/3 - 1/3 - 0$, $1 - 2/5 - 0$, and $1 - 3/7 - 0$. Upstream neutral modes at the upper, positively gated interface, accompany the co-propagating interface charge modes (see Figure 1 and schematic in S7), partly suppressing the visibility (to around 2-10%). The two QPCs were initially tuned to partition the innermost interface mode in all three configurations, i.e., the one carrying $1/3$, $1/15$, and $1/35$ (in units of the quantum conductance), with an average transmission between S1 and D1 of the OMZI kept at $t_{\text{S1-D1}} = 0.8$ at $\nu_b = 1/3$ and $t_{\text{S1-D1}} = 0.5$ at $\nu_b = 2/5$ and $3/7$.

The flux periodicities in the three configurations matched the expectations based on the partitioned fractional charges at the two QPCs. Figure 2 shows the observed interference patterns with $V_{\text{TG}} = 0$ in the three configurations with the inner mode partitioned. The actual inner area of the OMZI is not known (being depleted near the $\nu = 0$ side and accumulated near the

accumulated side); it likely deviates from the fabricated one (by some ~5-10% from $3\mu\text{m}^2$), and also depends on ν_b . Hence, for $\nu_b=1/3$, $\nu_b=2/5$, $\nu_b=3/7$, assuming the fabricated area would lead to non-integer periodicities: $\sim 3.5\Phi_0$, $\sim 5.5\Phi_0$, and $\sim 6.5\Phi_0$. However, assuming deviations from the fabricated area, the quantized periodicities are consistent with: $\sim 3\Phi_0$ (actual area $2.6\mu\text{m}^2$), $\sim 5\Phi_0$ (actual area $2.76\mu\text{m}^2$), and $\sim 7\Phi_0$ (actual area $3.2\mu\text{m}^2$). The periodicities in V_{MG} obey $B \times \Delta V_{\text{MG}}^i = 85 \pm 3$ Tesla-mV, agreeing with a constant ‘gate – 2DEG’ capacitance. As anticipated, the B - V_{MG} pajamas are free of phase slips. It is worth noting that interference of integer modes failed due to a lack of partitioning in the QPCs due to the opposite spins of the co-propagating interface modes.

The theoretically expected braiding phases for Jain states have been obtained in several studies [[\(9\)](#), [\(13\)](#), [\(7, 27, 38, 39\)](#), and in [S2](#)]. These incompressible FQH states arise at fractional fillings $\nu = \frac{n}{2pn+1}$, with the integer n denoting the number of filled composite fermion (CF) levels and p the CF generation. Here, $p=1$ corresponds to two-flux quantum CFs. Elementary QPs of the Jain states carry a fractional charge, $e^* = \frac{e}{2pn+1}$ and obey fractional statistics. Exchanging two QPs yields a phase factor $\pm \frac{2\pi}{2pn+1}$, depending on the orientation of the exchange path. The two paths of the OMZI differ by a full loop around the interferometer center and acquire a quantized phase difference of $\theta^* = \frac{2}{2pn+1}$ for each localized QP. Here, we consider the fillings, $\frac{1}{3}, \frac{2}{5}, \frac{3}{7}$, with the expected braiding phases $\theta^* = \frac{2}{3}, \frac{2}{5}, \frac{2}{7}$ in units of 2π (see [S2](#)).

To observe these braiding phases, we measured the AB pajamas at non-zero top-gate voltage in the range $V_{\text{TG}} = -(50-100)$ mV for all three filling configurations, with the QPCs tuned to partition the **innermost** edge mode in each configuration. The observed quantized phase slips ([Figure 3](#)) are expected to take place approximately when the magnetic flux, which pierces the actual depleted area under the top gate, changes by $1\Phi_0$ (independent of V_{MG}). The magnitudes of the discrete phase slips are determined either by direct observation of the 2D pajama plots or by using the ‘lock in’ procedure (described briefly in the Methods Section and, in more detail, in [S3](#)). The magnitudes of the phase slips noted in [Figure 3](#) generally agree with the expected ones.

Surprisingly, the signs of the flips (modulo 2π) at the fillings $\nu=\frac{2}{5}$ and $\nu = \frac{3}{7}$ are opposite to the expectations. An increasing magnetic field reduces the filling factor, which is expected to create quasi-holes inside the interferometer. Instead, the observed phase jumps at $\nu = \frac{2}{5}$ and $\nu= \frac{3}{7}$ correspond to added quasiparticles. Studies of the interfering outer modes and the corresponding phase slips are presented in Section [S7](#).

The most striking observation of anyonic braiding in the OMZI occurs when B and V_{MG} are held constant, allowing the AB phase to remain unchanged while varying the top-gate voltage, V_{TG} . This process introduces QPs into the center without disturbing the interference pattern, enabling precise detection of phase slips. This test was performed in the configurations. $\nu_b=1/3$ and $\nu_b=2/5$. A 2D plot of the OMZI conductance as a function of V_{TG} and B is shown in [Figure 4](#) (a different pajama type). At a constant magnetic field near a conductance step, a minute voltage change of the TG ($\Delta V_{TG}\sim 1\text{mV}$) leads to a sharp jump in the conductance of the OMZI ([Figure 4](#)). To translate the conductance steps to a phase slip in the AB interference, [Figures 4b & 4d](#) show the AB oscillations (as a function of B , on both sides of vertical dashed lines that mark the conductance steps). The abrupt shift in the AB oscillations as a function of B (over $\Delta V_{TG}=1\text{mV}$) directly reveals the quantized phase change due to added QPs at the TG. The detailed phase slips are provided in captions of [Figure 4](#).

Our experiments demonstrate the robust detection of anyonic braiding in fractional quantum Hall states using a novel optical-like Mach-Zehnder design (OMZI). The OMZI's co-propagating interface modes eliminate Coulomb charging effects and avoid interference area breathing due to the magnetic field. As a result, the OMZI can observe either pristine Aharonov-Bohm oscillations or purely anyonic braiding phases, depending on its mode of operation. An added top-gate controls a floating island in the interferometer's center, allowing exciting localized quasiparticles on demand by tuning the TG voltage. Changing V_{TG} does not affect the OMZI's AB interference parameters and thus allows direct observations of quasiparticle braiding phases. The OMZI's geometry requires only small modifications to realize different probes of quasiparticle statistics, such as time braiding ([11](#), [12](#)) and HOM experiments of quasiparticles ([40](#)).

This versatility makes the OMZI an ideal tool for obtaining interference and braiding phases of non-Abelian FQH states.

Methods

Sample fabrication process

The MESA of the device, with dimensions $250 \times 650 \mu\text{m}^2$ was prepared in GaAs/AlGaAs heterostructure by wet etching in $H_2O_2: H_3PO_4: H_2O = 1:1:50$ for 100 seconds. The 2DEG depth was 170 nm from the surface. The ohmic contacts were deposited at the edge of the mesa as well as within the MESA (for the interface modes) in a sequence, Ni (15 nm), Au (260 nm), Ge (130 nm), Ni (87.5 nm), Au (15 nm) from the top GaAs surface. This process was followed by annealing at 440°C for 80 seconds. The sample was covered by 30 nm of HfO_2 layer to electrically separate the ohmic contacts from the large metal gates (Ti (5 nm)/Au (15 nm)). Two large metal gates separated the MESA into three regions with filling factors, ν_u, ν_b, ν_l . In the following step, the MESA was covered again by 25 nm HfO_2 layer, followed by the deposition of QPCs, the modulation gate (MG), and the top gate (TG). In the final step, ohmic contacts, large metallic gates, QPCs, and MG were connected to pads via thick gold lines. The TG was connected by an *air bridge* in the interferometer region, followed by gold lines that passed over the HfO_2 that coated the metallic gates.

Geometric phase analysis

The phase slips are analyzed using the spatial lock-in method. Namely, the Aharonov-Bohm oscillations described by $T(\mathbf{r}) = A(\mathbf{r})\sin(\mathbf{q}\mathbf{r} + \theta(\mathbf{r}))$, where $\mathbf{r} = (B, V)$, $\mathbf{q} = (q_B, q_V)$ is the frequency of the AB oscillations and the $\theta(\mathbf{r})$ is the phase shift due to the phase slips. To extract $\theta(\mathbf{r})$, two lock-in signals are defined $s_1(\mathbf{r}) = \cos(\mathbf{q}\mathbf{r})$ and $s_2(\mathbf{r}) = \sin(\mathbf{q}\mathbf{r})$. The original signal $T(\mathbf{r})$ is multiplied by these signals, and low-pass filtering is applied to obtain outputs proportional to $\sin \theta(\mathbf{r})$ and $\cos \theta(\mathbf{r})$. The ratio of these allows us to calculate the phase slips as $\theta(\mathbf{r}) =$

$$\arctan \frac{LPF(s_1(\mathbf{r}) \times T(\mathbf{r}))}{LPF(s_2(\mathbf{r}) \times T(\mathbf{r}))}.$$

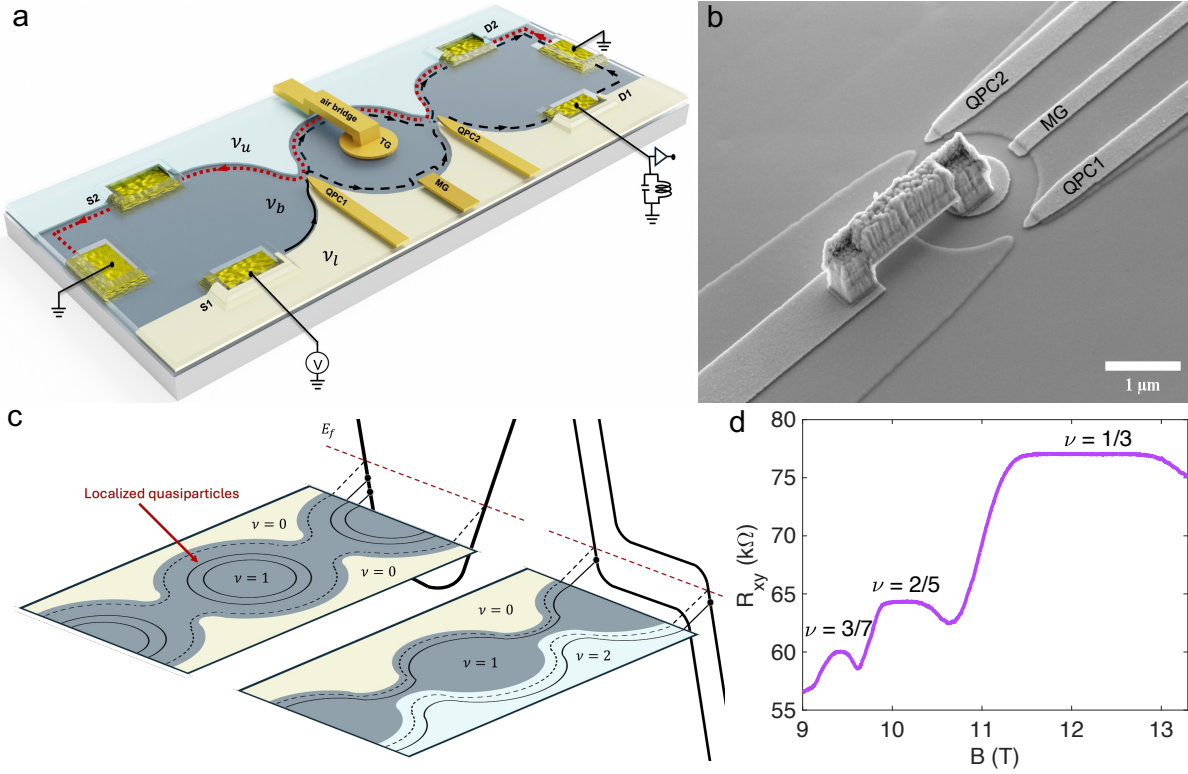


Figure 1. Optical-like MZI (OMZI) vs FPI.

(a) A schematic of the OMZI. The lower gate (light yellow with filling factor ν_l) is biased negatively, depleting the density. The upper gate (light blue with filling factor ν_u) is biased positively, increasing the density. Co-propagating modes (downstream in grey) are partitioned at QPC1 and QPC2. The source S1 is charged and the interfering signal is measured in D1. Upstream neutral modes are drawn in dotted red lines. An anti-dot in the middle of the OMZI bulk is formed by a negatively charged top-gate (TG) connected via an air bridge to a power supply. **(b)** An SEM micrograph of the OMZI. **(c)** A comparison between the FPI and the OMZI for integer quantum Hall states based on semiclassical electron trajectories. In the FPI (left) states below the Fermi level E_f form closed orbits corresponding to localized quasiparticles. Fully or partially closed trajectories suffer from Coulomb interactions. In the OMZI (right), all trajectories extend beyond the central region and are insensitive to charging effects. **(d)** The Hall resistance is in the range of the fractional states under study.

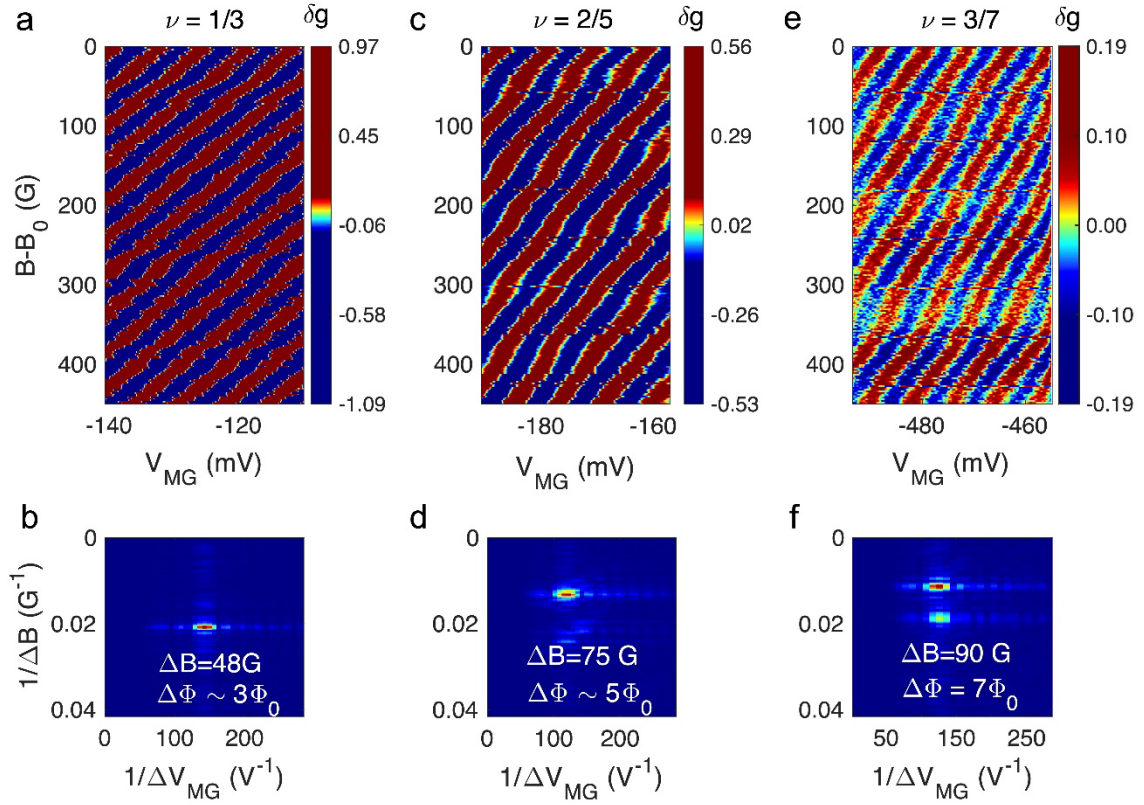


Figure 2. Aharonov Bohm pajamas plot of co-propagating edge modes in an optical-like MZI.

The 2d Aharonov-Bohm interference in the OMZI (AB pajamas), as a function of magnetic field B and the modulation-gate voltage V_{MG} . The pajamas in **a**, **c**, and **e** correspond to the partitioned *innermost* modes that carry the quasiparticles (QPs), $e/3$, $e/5$, and $e/7$. The FFTs in **b**, **d**, and **f** reflect the expected periodicities. $\Delta\Phi = (e/e^*)\Phi_0$. Phase slips related to QP excitations are absent, as expected.

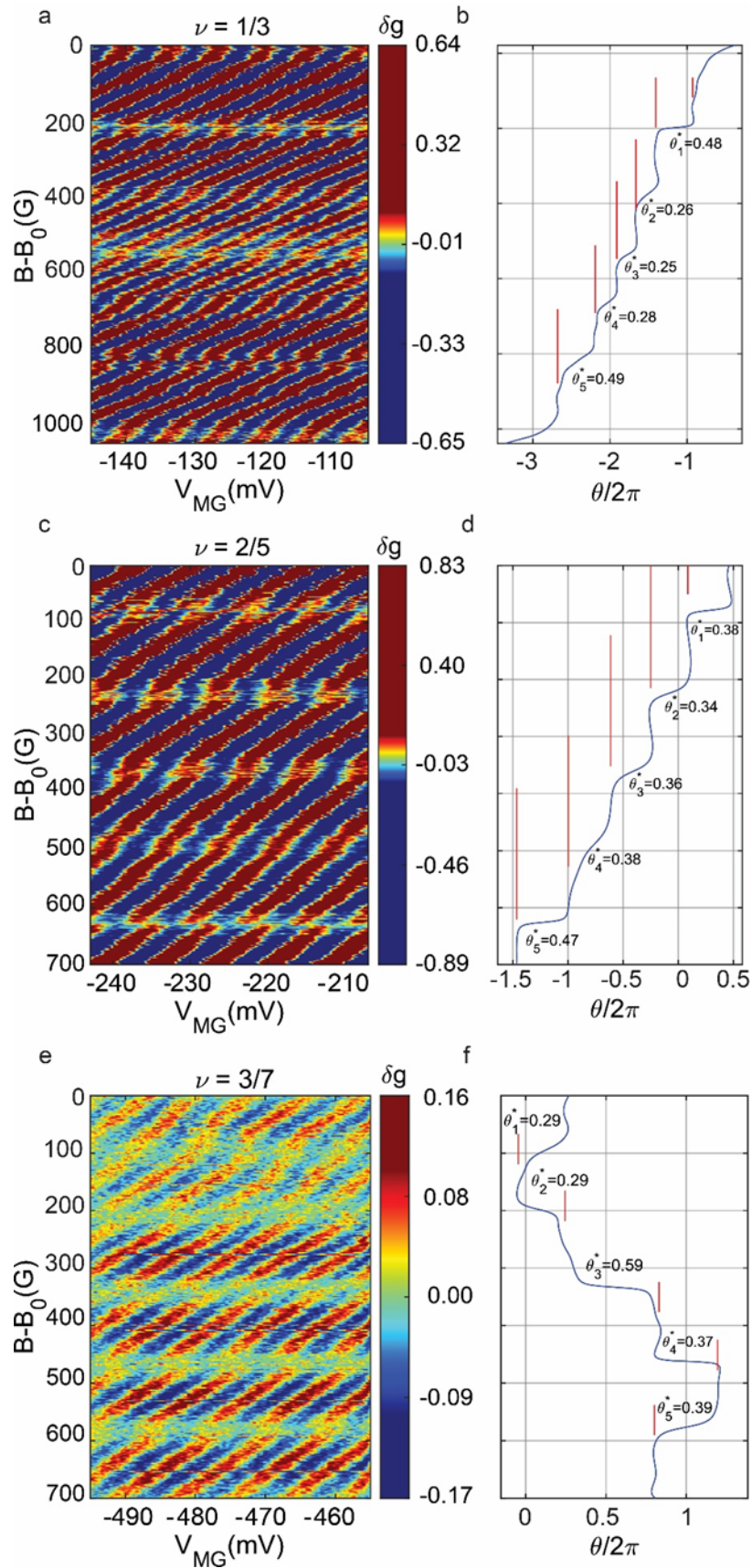


Figure 3. Aharonov Bohm pajama with magnetic field excitations of local quasiparticles.

Figures **a**, **c**, and **e** show the 2D Aharonov-Bohm interference as a function of B and V_{MG} (AB pajama), while the top gate (TG) of the anti-dot is biased in the range -50mV to -100mV (leading to slight depletion under the gate). Clear phase slips appear for approximately every *flux quantum* piercing the ‘effective area’ under the TG. The fabricated area of the TG is $0.78\mu\text{m}^2$; however, the effective area extracted from the distance between phase jumps is $0.27\mu\text{m}^2@v_b=1/3$; $0.3\mu\text{m}^2@v_b=2/5$, and $0.34\mu\text{m}^2@v_b=3/7$, suggesting a smaller depleted island under the top gate.

Figures **b**, **d**, and **f** present the calculated phase slips with the Lock-In technique (see **Methods** and **S3** in the Supplementary Section). Red lines indicate the regions of constant phase and $\theta_1^*, \theta_2^*, \theta_3^*, \theta_4^*, \theta_5^*$ are phase shifts between two consecutive regions. The magnitudes of the phase slips (modulo 2π) generally agree with the theoretically expected value $\theta^* = \frac{2p}{1+2np}$, see **Table 1** in **S2**. At $v_b=1/3$, all phase jumps are consistent with the expected creation of quasi-holes as the magnetic field increases. Surprisingly, the jumps at $v_b=2/5$ jumps instead correspond to inserted quasiparticles. At $v_b=3/7$, both types of phase jumps are present.

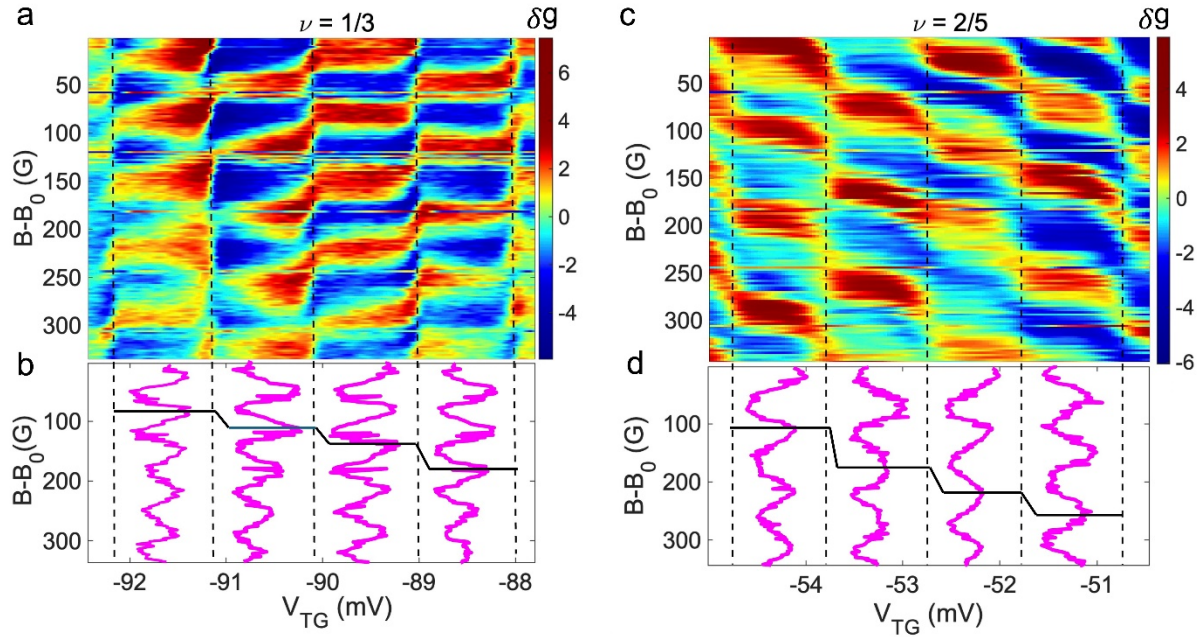


Figure 4. Local excitation of quasiparticles by activating the local anti-dot top gate.

A 2D plot of the Aharonov-Bohm interference with partitioning the innermost edge mode as a function of the magnetic field, B , and the top-gate voltage V_{TG} , for $\nu_b=1/3$ and $\nu_b=2/5$. As a function of V_{TG} , while keeping $B=\text{constant}$ (vertical dotted lines), an excitation of local QPs in the anti-dot takes place, leading to sharp phase jumps ($@\Delta V_{TG}=1\text{mV}$). The phase jumps shown in (a, b) are $\theta^* = 0.38 @ \nu_b=1/3$ for $e/3$ QPs, those in (c, d) are $\theta^* = 0.42 @ \nu_b=2/5$ for $e/5$ QPs. The visibility for $\nu_b=3/7$ is very low and does not yield reliable data (see expected θ^* @ S2, Table 1).

References

Uncategorized References

1. B. I. Halperin, Quantized Hall conductance, current-carrying edge states, and the existence of extended states in a two-dimensional disordered potential. *Physical Review B* **25**, 2185-2190 (1982).
2. R. dePicciotto *et al.*, Direct observation of a fractional charge. *Nature* **389**, 162-164 (1997).
3. M. Reznikov, R. de Picciotto, T. G. Griffiths, M. Heiblum, V. Umansky, Observation of quasiparticles with one-fifth of an electron's charge. *Nature* **399**, 238-241 (1999).
4. L. Saminadayar, D. C. Glattli, Y. Jin, B. Etienne, Observation of the $e/3$ fractionally charged Laughlin quasiparticle. *Physical Review Letters* **79**, 2526-2529 (1997).
5. F. Wilczek, Magnetic-Flux, Angular-Momentum, and Statistics. *Physical Review Letters* **48**, 1144-1146 (1982).
6. D. Arovas, J. R. Schrieffer, F. Wilczek, FRACTIONAL STATISTICS AND THE QUANTUM HALL-EFFECT. *Physical Review Letters* **53**, 722-723 (1984).
7. B. I. Halperin, Statistics of Quasiparticles and the Hierarchy of Fractional Quantized Hall States. *Physical Review Letters* **52**, 1583-1586 (1984).
8. J. M. Leinaas, J. Myrheim, On the theory of identical particles. *Il Nuovo Cimento B (1971-1996)* **37**, 1-23 (1977).
9. A. Stern, Anyons and the quantum Hall effect - A pedagogical review. *Annals of Physics* **323**, 204-249 (2008).
10. C. D. C. Chamon, D. E. Freed, S. A. Kivelson, S. L. Sondhi, X. G. Wen, Two point-contact interferometer for quantum Hall systems. *Physical Review B* **55**, 2331-2343 (1997).
11. J.-Y. M. Lee *et al.*, Partitioning of diluted anyons reveals their braiding statistics. *Nature* **617**, 277-281 (2023).
12. C. Han, J. Park, Y. Gefen, H. S. Sim, Topological vacuum bubbles by anyon braiding. *Nature Communications* **7**, 11131 (2016).
13. G. S. Jeon, K. L. Graham, J. K. Jain, Berry phases for composite fermions: Effective magnetic field and fractional statistics. *Physical Review B* **70**, 125316 (2004).
14. J. K. Jain, S. A. Kivelson, D. J. Thouless, Proposed measurement of an effective flux quantum in the fractional quantum Hall effect. *Physical Review Letters* **71**, 3003-3006 (1993).
15. N. Ofek *et al.*, Role of interactions in an electronic Fabry–Perot interferometer operating in the quantum Hall effect regime. *Proceedings of the National Academy of Sciences* **107**, 5276-5281 (2010).
16. Y. M. Zhang *et al.*, Distinct signatures for Coulomb blockade and Aharonov-Bohm interference in electronic Fabry-Perot interferometers. *Physical Review B* **79**, 241304 (2009).
17. R. Schuster *et al.*, Phase measurement in a quantum dot via a double-slit interference experiment. *Nature* **385**, 417-420 (1997).
18. B. Rosenow, S. H. Simon, Telegraph noise and the Fabry-Perot quantum Hall interferometer. *Physical Review B* **85**, 201302 (2012).
19. I. P. Levkivskiy, J. Fröhlich, E. V. Sukhorukov, Theory of fractional quantum Hall interferometers. *Physical Review B* **86**, 245105 (2012).
20. Y. Ji *et al.*, An electronic Mach-Zehnder interferometer. *Nature* **422**, 415-418 (2003).
21. I. Neder, M. Heiblum, Y. Levinson, D. Mahalu, V. Umansky, Unexpected behavior in a two-path electron interferometer. *Physical Review Letters* **96**, 016804 (2006).
22. I. Neder *et al.*, Interference between two indistinguishable electrons from independent sources. *Nature* **448**, 333-337 (2007).

23. B. I. Halperin, A. Stern, I. Neder, B. Rosenow, Theory of the Fabry-Perot quantum Hall interferometer. *Physical Review B* **83**, 155440 (2011).
24. J. Nakamura *et al.*, Aharonov–Bohm interference of fractional quantum Hall edge modes. *Nature Physics* **15**, 563-569 (2019).
25. I. Sivan *et al.*, Observation of interaction-induced modulations of a quantum Hall liquid's area. *Nature Communications* **7**, 12184 (2016).
26. J. Nakamura, S. Liang, G. C. Gardner, M. J. Manfra, Direct observation of anyonic braiding statistics. *Nature Physics* **16**, 931-936 (2020).
27. J. Kim *et al.*, Aharonov–Bohm interference and statistical phase-jump evolution in fractional quantum Hall states in bilayer graphene. *Nature Nanotechnology*, (2024).
28. N. L. Samuelson *et al.*, Anyonic statistics and slow quasiparticle dynamics in a graphene fractional quantum Hall interferometer. 2024 (10.48550/arXiv.2403.19628).
29. T. Werkmeister *et al.*, Anyon braiding and telegraph noise in a graphene interferometer. 2024 (10.48550/arXiv.2403.18983).
30. N. Byers, C. N. Yang, Theoretical considerations concerning quantized magnetic flux in superconducting cylinders. *Physical Review Letters* **7**, 46 (1961).
31. S. Kivelson, Semiclassical theory of localized many-anyon states. *Physical Review Letters* **65**, 3369-3372 (1990).
32. D. E. Feldman, Y. Gefen, A. Kitaev, K. T. Law, A. Stern, Shot noise in an anyonic Mach-Zehnder interferometer. *Physical Review B* **76**, 085333 (2007).
33. K. T. Law, D. E. Feldman, Y. Gefen, Electronic Mach-Zehnder interferometer as a tool to probe fractional statistics. *Physical Review B* **74**, 045319 (2006).
34. H. K. Kundu, S. Biswas, N. Ofek, V. Umansky, M. Heiblum, Anyonic interference and braiding phase in a Mach-Zehnder interferometer. *Nature Physics* **19**, 515-521 (2023).
35. E. V. Deviatov, S. V. Egorov, G. Biasiol, L. Sorba, Quantum Hall Mach-Zehnder interferometer at fractional filling factors. *Europhysics Letters* **100**, 67009 (2012).
36. N. Batra, Z. Wei, S. Vishveshwara, D. E. Feldman, Anyonic Mach-Zehnder interferometer on a single edge of a two-dimensional electron gas. *Physical Review B* **108**, L241302 (2023).
37. S. Biswas, H. K. Kundu, V. Umansky, M. Heiblum, Electron Pairing of Interfering Interface-Based Edge Modes. *Physical Review Letters* **131**, 096302 (2023).
38. G. S. Jeon, K. L. Graham, J. K. Jain, Fractional Statistics in the Fractional Quantum Hall Effect. *Physical Review Letters* **91**, 036801 (2003).
39. W. P. Su, Statistics of the fractionally charged excitations in the quantum Hall effect. *Physical Review B* **34**, 1031-1033 (1986).
40. C. K. Hong, Z. Y. Ou, L. Mandel, Measurement of subpicosecond time intervals between two photons by interference. *Physical Review Letters* **59**, 2044-2046 (1987).

Acknowledgments

M.H. thanks Dima E. Feldman for the fruitful discussions and Mitali Banerjee for her suggestions. B.G and M.L. thanks Arup Kumar Paul, H.K. Kundu and S. Biswas for the helpful comments that improved our device. D.F.M. acknowledges many illuminating conversations on quantum Hall interferometry with Yuval Ronen. D.F.M. was supported by the Israel Science Foundation (ISF) under Grant No. 2572/21 and by the Deutsche Forschungsgemeinschaft (DFG) within the CRC network TR 183 (project Grant No. 277101999). M.H. acknowledges the support of the European

Research Council under the European Union's Horizon 2020 research and innovation program (Grant Agreement No. 833078). M.L. thanks the Ariane de Rothschild Women Doctoral Program for their support.

Supplementary Material

S1. Quasiparticles in Fabry Perot and optical-like Mach Zehnder interferometers

Fractional quantum Hall (FQH) interferometers probe bulk properties such as quasiparticle charges and statistics using edge states. Quasiparticles in the bulk are well-defined, manifesting as local finite-energy excitations with a quantized charge. In contrast, the gapless edges permit excitations of arbitrary charge. To bridge the conceptual difference, adopting a shared language to describe both bulk and edge properties is helpful.

The boundary of any fractional quantum Hall state at filling factor ν supports a charge mode, i.e., a phase field ϕ governed by the Hamiltonian, $H_{\text{edge}} = u \int dx (\partial_x \phi)^2$. This mode encodes the charge density on the edge via $\rho = \frac{1}{2\pi} \partial_x \phi$, in units of the electron charge. A *finite* quantum Hall droplet of electrons can only carry an integer charge. Consequently, the total charge on the edge, which is given by the winding of ϕ in units of 2π , i.e., $Q = \frac{1}{2\pi} \int dx \partial_x \phi$ is an integer for any ν , unless the droplet's bulk contains quasiparticles. In systems with multiple boundaries (e.g., inner and outer edges in the Corbino geometry), the total charge on all edges, $Q \equiv \sum_i Q_i$ is quantized as an integer. By contrast, the charges Q_i on individual edges can change in steps of the fundamental quasiparticle charge e^* .

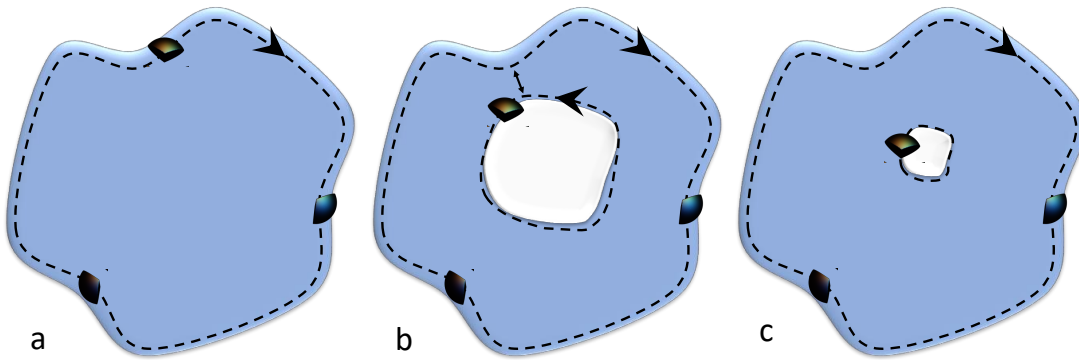


Figure S1: Quasiparticles in a fractional quantum Hall droplet. (a) The gapless edge of an FQH droplet supports arbitrarily charged excitations, provided the total charge is an integer. (b) Quasiparticles with fractional charge e^* can transfer between the inner and the outer edge, similar to a quantum point contact (QPC) (c) Shrinking the inner region to a point when the inner edge carries fractional charge results in a bulk quasiparticle.

Bulk quasiparticles can be described as edge modes encircling a small region of altered filling factor (Figure S1). Consider a small ‘anti-dot’ region with zero filling, much smaller than the quantum Hall droplet. This system realizes the Corbino geometry, with an outer edge mode encircling the droplet and an inner edge around the anti dot. The states on the inner edge are

subject to finite size quantization, meaning their energy levels are discrete. Varying the magnetic field, electron density, or the anti dot area continuously changes these energies. When it becomes favorable, a fractional charge e^* transfers from the droplet's outer (longer) edge to the periphery of the anti dot. The fractional charge on the inner edge is equivalent to a bulk quasiparticle. Specifically, slowly shrinking a well-isolated anti dot to a point does not change charge or statistics, which are quantized. Once the anti dot has been fully removed, a bulk quasiparticle remains.

This analysis holds even when the anti dot's filling factor is non-zero. If the anti dot realizes a fractional quantum Hall state at a filling factor ν' , the total charge in its vicinity is still quantized according to the surrounding bulk. If that charge had a different fractional value, shrinking the dot to zero would leave behind a finite energy excitation with a charge not supported by the quantum Hall bulk, creating a contradiction. In terms of the edge modes, the anti-dot at filling ν' creates an additional charge mode at its perimeter. Since the anti dot only has a single (outer) boundary, this additional mode can only carry an integer charge (i.e., 2π windings), while the bulk's inner mode permits $2\pi e^*$ windings. The two combine into a total charge mode with $2\pi e^*$ windings at the perimeter of the anti-dot. Therefore, the total charge localized near the anti dot remains quantized at e^* , dictated by the surrounding bulk at filling ν . If the anti-dot supports fractional charges $e'^* \neq e^*$, the charges only exist as neutral 'quasiparticle—quasihole' pairs, which do not contribute to the braiding phase.

The central region of a Fabry Perot Interferometer (FPI) behaves similarly to an anti dot, with the outside regions of the FPI acting as the bulk. Changes in the magnetic field or area affect the number of quasiparticles (edge-mode excitations) localized along the FPI's inner periphery, as shown by the closed loops in Fig. 1(c). However, unlike in an isolated anti-dot, the edge states couple to the states extending beyond the central part of the FPI, reducing their lifetime. The introduction of localized quasiparticles with a magnetic field and their coupling to the outside modes are intrinsic properties of FPIs and require careful treatment. By contrast, these effects are absent in both the standard and the optical-like Mach Zehnder Interferometers.

In the optical-like Mach Zehnder Interferometer (OMZI), all charge modes co-propagate and do not support localized states in the central region [Fig. 1(c)]. This desirable feature comes at the cost of only displaying AB phases without anyonic braiding contributions (Fig. 2). To observe the latter; quasiparticles must be introduced through a different mechanism, such as a top gate defining an anti dot. Varying the voltage on the anti dot introduces quasiparticles, which transfer from the outer edge. Alternatively, changing the magnetic field alters the bulk filling factor and introduces quasiparticles that can either be delocalized on the outer edge or localized at the anti-dot. As a rule of thumb, localized particles are expected to appear whenever the magnetic flux through the anti-dot area changes by one flux quantum. Since this area is much smaller than the center of the interferometer, quasiparticles are introduced at a reduced rate compared to that in the FPI. Moreover, these quasiparticles are well isolated from the interfering modes.

S2. Braiding phases of Abelian quasiparticles

The statistical properties of quasiparticles in Abelian quantum Hall states orders are efficiently captured using the K-matrix formalism [1]. An integer-valued matrix K and a charge vector \mathbf{t} encode a state at bulk filling factor $\nu = \mathbf{t}^T K^{-1} \mathbf{t}$, whose vacuum interface is described by the Lagrangian

$$L = \frac{1}{4\pi} \sum_{i,j} \partial_x \phi_i (K_{ij} \partial_t \phi_j - V_{ij} \partial_x \phi_j),$$

with a non-universal velocity matrix V . All bulk quasiparticles of the topological order (K, \mathbf{t}) are specified by integer vectors \mathbf{l} with the electric charge given by

$$Q(\mathbf{l}) = \mathbf{t}^T K^{-1} \mathbf{l}. \quad (1)$$

Fully encircling one quasiparticle defined by \mathbf{l}_1 by another defined by \mathbf{l}_2 yields the braiding phase

$$\theta(\mathbf{l}_1, \mathbf{l}_2) = 2\pi \mathbf{l}_1^T K^{-1} \mathbf{l}_2. \quad (2)$$

For Jain states at $\nu = \frac{n}{2pn+1}$, K is an $n \times n$ matrix, which can be expressed using the identity matrix and matrix of ones as

$$K = \begin{pmatrix} 1 & \cdots & 0 \\ \vdots & \ddots & \vdots \\ 0 & \cdots & 1 \end{pmatrix} + 2p \begin{pmatrix} 1 & \cdots & 1 \\ \vdots & \ddots & \vdots \\ 1 & \cdots & 1 \end{pmatrix}, \quad (3)$$

with n –component charge vector $\mathbf{t} = (1, \dots, 1)$. Inverting Eq. (3) yields

$$K^{-1} = \begin{pmatrix} 1 & \cdots & 0 \\ \vdots & \ddots & \vdots \\ 0 & \cdots & 1 \end{pmatrix} - \frac{2p}{1+2np} \begin{pmatrix} 1 & \cdots & 1 \\ \vdots & \ddots & \vdots \\ 1 & \cdots & 1 \end{pmatrix}. \quad (4)$$

For a fundamental quasiparticle $\mathbf{l}_0 = (1, 0, 0, \dots)$, Eqs. (1) and (2) yield the known results for Jain states,

$$Q(\mathbf{l}_0) = \frac{1}{1+2np},$$

$$\theta(\mathbf{l}_0, \mathbf{l}_0) = 2\pi - 2\pi \frac{2p}{1+2np}.$$

[1] *Quantum Field Theory of Many-body Systems*, Xiao-Gang Wen (Oxford Graduate Text, 2004)

For the first Jain's states, $p = 1$. Ignoring the first 2π term, the reduced phase is: $\theta^* = \frac{2}{1+2n}$ (see above).

ν	n	$1 - \theta^*$, expectation	θ^* , from $B - V_{MG}$	θ^* , from $B - V_{TG}$
1/3	1	$1 - \frac{2}{3} = 0.33$	0.35 ± 0.11	0.38
2/5	2	$1 - \frac{2}{5} = 0.6$	0.39 ± 0.05	0.42
3/7	3	$1 - \frac{2}{7} = 0.71$	0.39 ± 0.11	-

Table 1. Comparison of the theoretically expected value $\theta^* = \frac{2}{1+2n}$ for the first three Jain fillings. Spatial lock-in method calculation of the 'pajamas' in Fig. 3 ($B - V_{MG}$); direct *phase jumps* from the B dependence across the top gate abrupt ΔV_{TG} change in Fig. 4 ($B - V_{TG}$).

S3. Phase slips analysis by spatial *lock-in method*

The main interference signal in the space of B and V_{MG} (and V_{TG}) is a periodic signal that can be described by:

$$T(\mathbf{r}) = A(\mathbf{r})\sin(\mathbf{q}\mathbf{r} + \theta(\mathbf{r})), \quad (1)$$

where $\mathbf{q} = (q_B, q_V)$ is the frequency of the Aharonov-Bohm oscillations, $\mathbf{r} = (B, V)$, and $\theta(\mathbf{r})$ is the additional phase that remains constant in the absence of the phase slips and increases stepwise after each phase slip by the value of the statistical phase, $\mathbf{r} = (B, V)$.

To extract the statistical phase term $\theta(\mathbf{r})$, we define the *lock-in signal*,

$$\begin{aligned} s_1(\mathbf{r}) &= \cos(\mathbf{q}\mathbf{r}) \\ s_2(\mathbf{r}) &= \sin(\mathbf{q}\mathbf{r}), \end{aligned} \quad (2)$$

multiplying the original signal $T(\mathbf{r})$ by s_1 and s_2 separately,

$$\begin{aligned} s_1(\mathbf{r}) \times T(\mathbf{r}) &= A(\mathbf{r})\cos(\mathbf{q}\mathbf{r})\sin(\mathbf{q}\mathbf{r} + \theta(\mathbf{r})) \\ &= \frac{A(\mathbf{r})}{2} (\sin(\mathbf{q}\mathbf{r} + \mathbf{q}\mathbf{r} + \theta) + \sin(\mathbf{q}\mathbf{r} + \theta - \mathbf{q}\mathbf{r})) \\ &= \frac{A(\mathbf{r})}{2} (\sin(2\mathbf{q}\mathbf{r} + \theta(\mathbf{r})) + \sin \theta(\mathbf{r})) \end{aligned} \quad (3)$$

$$\begin{aligned}
s_2(\mathbf{r}) \times T(\mathbf{r}) &= A(\mathbf{r}) \sin(\mathbf{q}\mathbf{r}) \sin(\mathbf{q}\mathbf{r} + \theta(\mathbf{r})) \\
&= \frac{A(\mathbf{r})}{2} (\cos(\mathbf{q}\mathbf{r} + \theta(\mathbf{r}) - \mathbf{q}\mathbf{r}) - \cos(\mathbf{q}\mathbf{r} + \theta(\mathbf{r}) + \mathbf{q}\mathbf{r})) \\
&= \frac{A(\mathbf{r})}{2} (\cos \theta(\mathbf{r}) - \cos(2\mathbf{q}\mathbf{r} + \theta(\mathbf{r})))
\end{aligned}$$

Finally, we add low-pass filtering (LPF) to the 'new signals',

$$\begin{aligned}
LPF(s_1(\mathbf{r}) \times T(\mathbf{r})) &= \frac{A(\mathbf{r})}{2} \sin \theta(\mathbf{r}) \\
LPF(s_2(\mathbf{r}) \times T(\mathbf{r})) &= \frac{A(\mathbf{r})}{2} \cos \theta(\mathbf{r})
\end{aligned} \tag{4}$$

$$\begin{aligned}
\frac{LPF(s_1(\mathbf{r}) \times T(\mathbf{r}))}{LPF(s_2(\mathbf{r}) \times T(\mathbf{r}))} &= \tan \theta(\mathbf{r}) \\
\theta(\mathbf{r}) &= \arctan \frac{LPF(s_1(\mathbf{r}) \times T(\mathbf{r}))}{LPF(s_2(\mathbf{r}) \times T(\mathbf{r}))}
\end{aligned} \tag{4}$$

In the figures below, a step-by-step illustration of the method is provided.

Step 1. Raw data of pajamas with phase slips (**Fig. 1**),

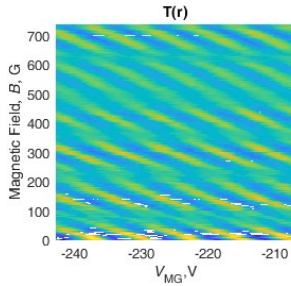


Fig. 1

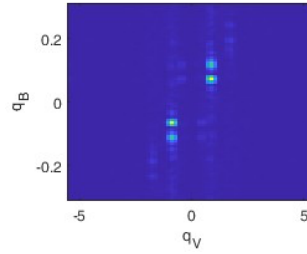
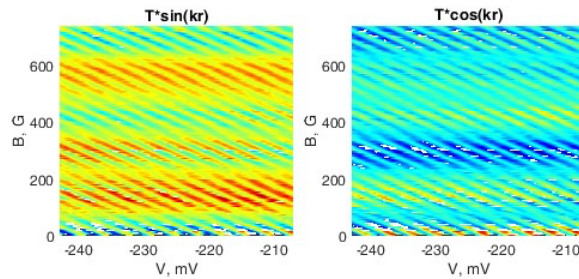


Fig. 2

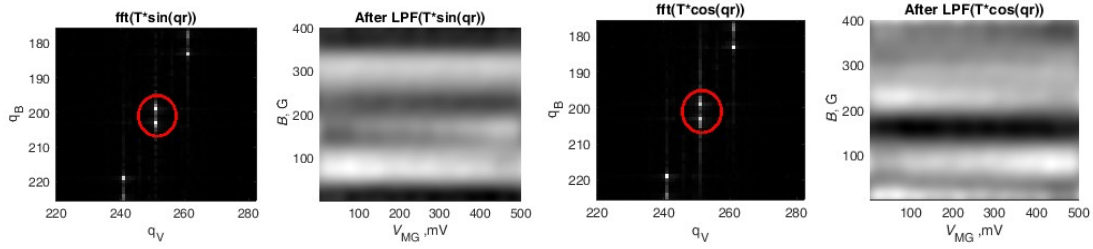
Step 2. Performing a *fast Fourier transform* to determine the spatial frequency \mathbf{q} (**Fig. 2**)

Since the frequency q_B is not a single sharp peak, the frequency \mathbf{q} used in the analysis is defined by choosing a frequency between the two visible peaks that best reflects the stepwise behavior of $\theta(\mathbf{r})$.

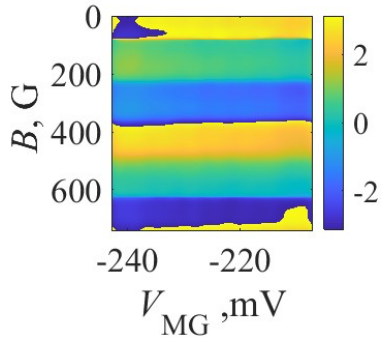
Step 3. Multiplication by s_1 and s_2



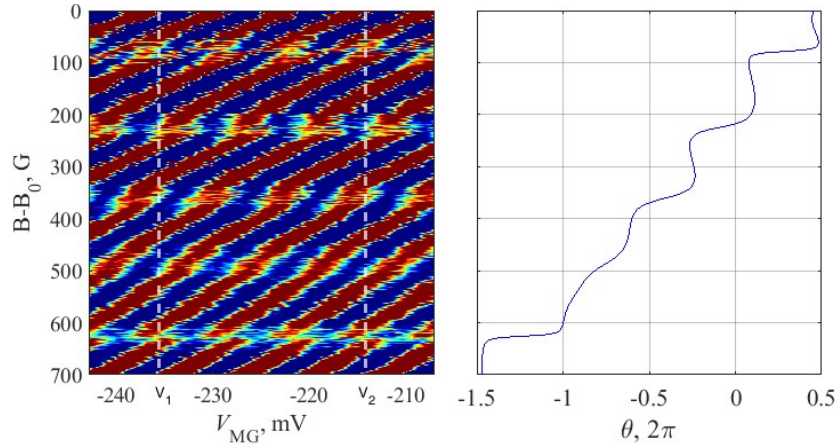
Step 4. Low-pass filtering



Step 5: Color plot of the $\theta(B, V_{mg})$



Step 6: Averaging in a range of voltages $V_1 < V < V_2$ (table 2).



V_{MG}, mV	$1/3$	$2/5$	$3/7$
V_1, mV	-106.2	-235.6	-465.0
V_2, mV	-105.0	-214.2	-455.3

Table 2. Voltage range for averaging the phase to get the result in Fig. 3 from the main text.

The spatial lock-in method is advantageous since it allows isolating of the phase slips associated with the specific frequency of Aharonov Bohm oscillations. It effectively captures the absolute value of each phase slip at the chosen frequency. It is less reliable for capturing the direction of the phase slip since the visibility during the phase jumps is significantly suppressed. In addition,

the Aharonov-Bohm frequency along the wide range of the magnetic field can be subject to slight change, which may lead to an error in defining the phase flip size.

An alternative method is to use a fast Fourier transform for each horizontal slice (fixed magnetic field) and look at the evolution of the complex phase along the magnetic field. This method might more accurately detect the frequency change along B axis. However, a linear correction is required to determine the phase slip, which is unnecessary in the abovementioned method.

S4. Interfacing Abelian fractional states

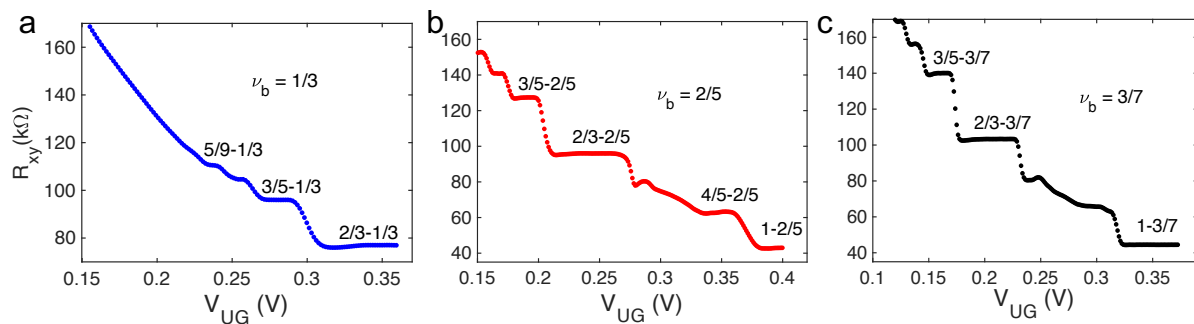


Figure S2: Interfacing Abelian fractional states. Two terminal resistance measurements at the interface between $\nu_u - \nu_b$. The bulk is fixed at $\nu_b = 1/3, 2/5, 3/7$, and the upper gate (UG) is swept with positive bias. Clear quantized plateaus corresponding to $\nu_u = 5/9, 4/7, 3/5$ and $2/3$ (a) $\nu_u = 3/5, 2/3, 4/5$ and 1 (b) $\nu_u = 3/5, 2/3$, and 1 (c); accurate to $\sim 1\%$ are observed. For $\nu_b = 2/5$, $\nu_u = 1$ corresponds to a 150% increase in the 2DEG density underneath the gate. After the charge has equilibrated, the ' $\nu_u - \nu_b$ ' interface charge mode is accompanied by upstream neutral modes.

S5: Interference of counter-propagating edge modes

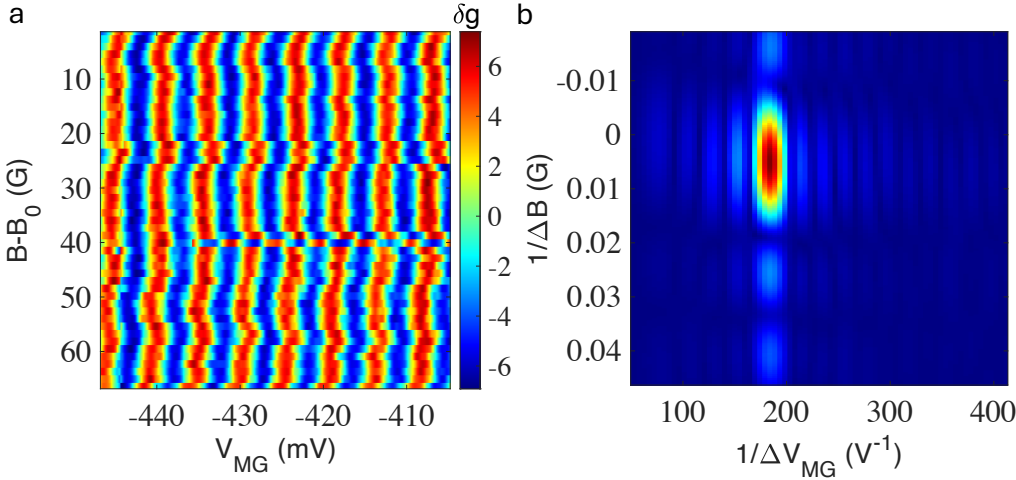


Figure S3: Interference in Fabry-Perot interferometer at $\nu=1/3$. (a) Transmission oscillation of the edge mode at $\nu=1/3$ in the 0-1/3-0 configuration. While the transmission is independent of the magnetic field B , it oscillates as a function of V_{MG} . This is a typical behavior of Coulomb-dominated (CD) interference. (b) 2D FFT gives the periodicity $\Delta V_{MG}=5.5$ mV.

S6: Dependence of flux periodicity on the interface edge mode on the population side

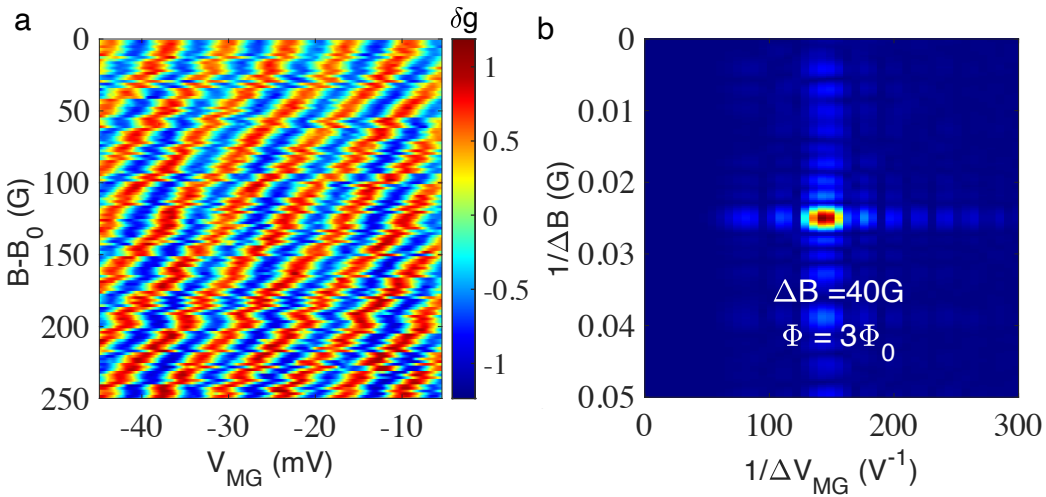


Figure S4: Aharonov Bohm pajama in optical-like MZI at $\nu=1/3$ (a) Conductance oscillation with the interfering 1/3 edge mode in the B - V_{MG} plane in the filling-factor configuration fillings: $5/9 - 1/3 - 0$. The top gate is fixed at $V_{TG}=0$ V. As anticipated, the pajama is free from phase flips. (b) 2D Fourier transforms of the pajamas plots showing a single peak. The periodicity in B is 40G and in V_{MG} is 7mV. The estimated AB area is $\sim 3 \mu\text{m}^2$, leading to a flux periodicity $3\Phi_0$.

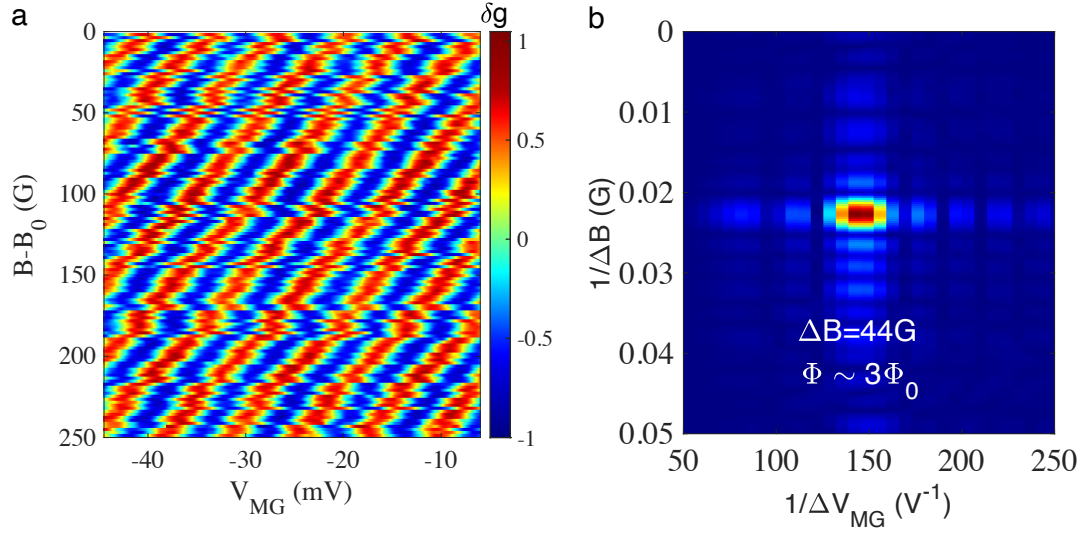


Figure S5: Aharonov Bohm pajama in optical like MZI at $\nu=1/3$ (a) Transmission oscillation with the interfering $1/3$ edge mode in the B - V_{MG} plane with a $3/5$ - $1/3$ - 0 configuration. The top gate (of the anti dot) is fixed at $V_{TG}=0$ V. The Pajama is free of phase jump. (b) 2D Fourier transforms of the pajama plot showing a single peak. The periodicity in B is 44 G and V_{MG} is 6.8 mV. The calculated AB area is $\sim 2.82 \mu\text{m}^2$, leading to a flux periodicity $\sim 3\Phi_0$. Similar results were observed in ' $2/3$ - $1/3$ - 0 ' (see main text), and ' $5/9$ - $1/3$ - 0 ' (Figure S4) and for an outer partitioned $1/3$ mode in the ' 1 - $2/5$ - 0 ' configuration (Figure S7), suggesting flux periodicity is solely determined by the QPC filling and independent of ν_u .

S7: Interference of outer edge modes in an optical-like MZI

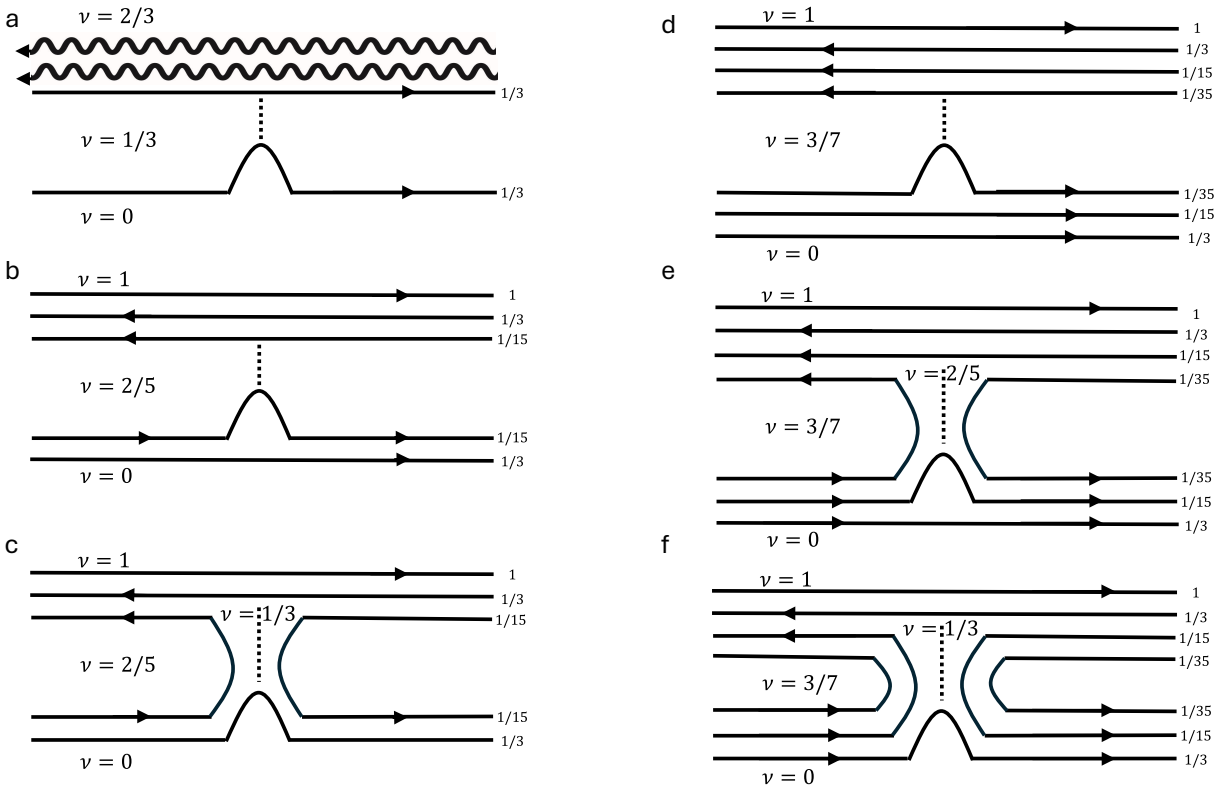


Figure S6: Edge mode partitioning in the co-propagating QPC. The filling factor inside the QPC determines the Aharonov Bohm flux periodicity and the statistical phase slip in the respective interferometer. The solid lines are charged modes and the wavy lines are neutral modes. (a) Partitioning the $1/3$ mode: $\nu_{\text{bulk}} = 1/3$, $\nu_{\text{qpc}} = 1/3$ (b) Partitioning the inner $1/15$ mode: $\nu_{\text{bulk}} = 2/5$, $\nu_{\text{qpc}} = 2/5$ (c) Partitioning the outer $1/3$ mode: $\nu_{\text{bulk}} = 2/5$, $\nu_{\text{qpc}} = 1/3$ (d) Partitioning the inner $1/35$ mode: $\nu_{\text{bulk}} = 3/7$, $\nu_{\text{qpc}} = 3/7$ (e) Partitioning the middle $1/15$ mode: $\nu_{\text{bulk}} = 3/7$, $\nu_{\text{qpc}} = 2/5$ (f) Partitioning the outer $1/3$ mode: $\nu_{\text{bulk}} = 3/7$, $\nu_{\text{qpc}} = 1/3$.

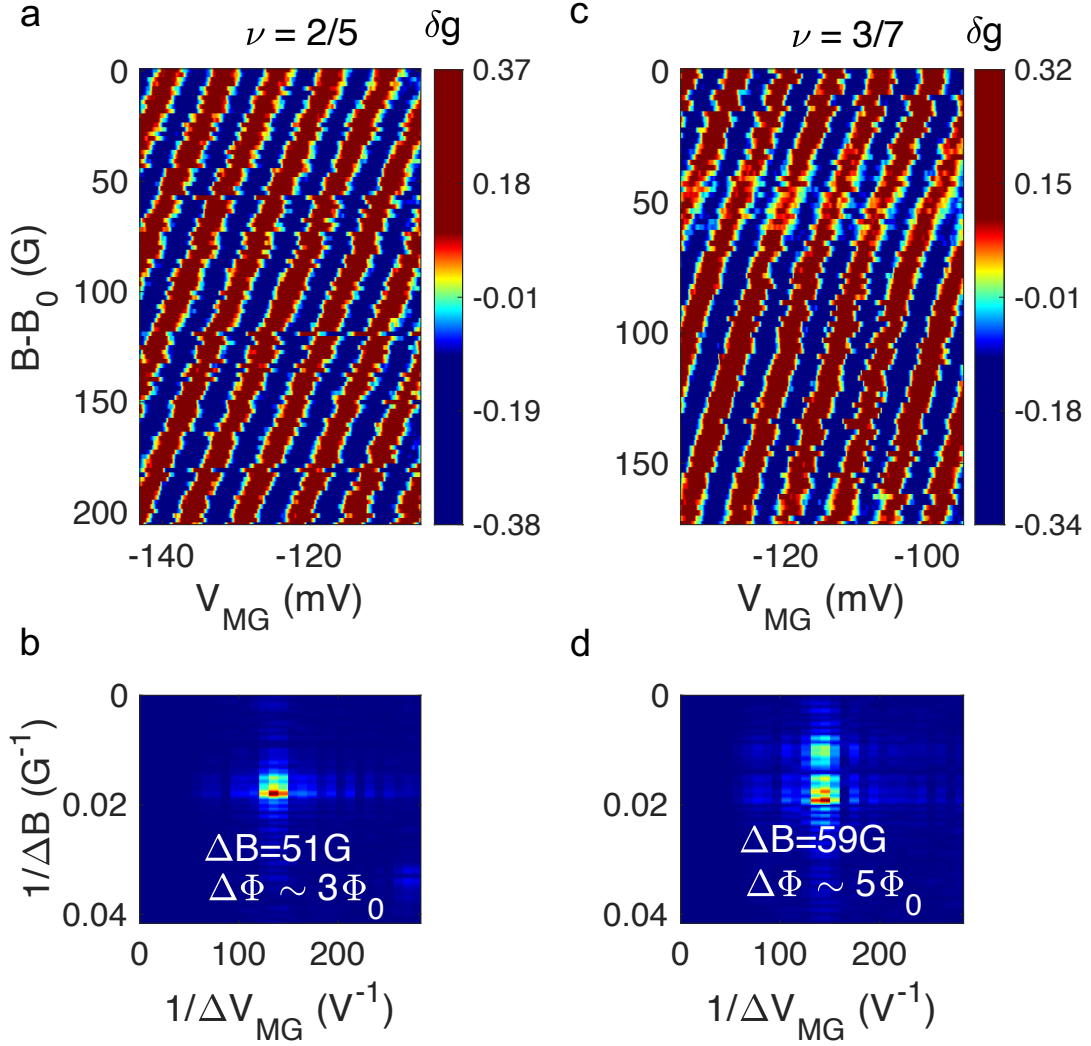


Figure S7: Aharonov Bohm pajamas of the co-propagating outer edge mode for the bulk filling $\nu_u=2/5$ and $\nu_u=3/7$. For these measurements, the QPCs are biased to achieve 90% transmission of the outer 1/3 mode (or the 1/15 mode) of the bulk with filling factor 2/5 (or 3/7). Top gate (TG) is kept at $V_{TG}=0V$. Within the tolerable voltage limit of the QPCs, we could not partition the outer 1/3 mode of the $\nu=3/7$ bulk. The color scale shows conductance oscillation with clear periodicities corresponding to different QPC filling: $3\Phi_0$ (a,b) and $5\Phi_0$ (c,d). The estimated AB area for the outer mode of $\nu=2/5$ is $\sim 2.45 \mu\text{m}^2$, and for the middle edge of $\nu=3/7$ is $\sim 3.5 \mu\text{m}^2$. As explained in the main text, the small area correction depends on the pinching voltage of the QPC.

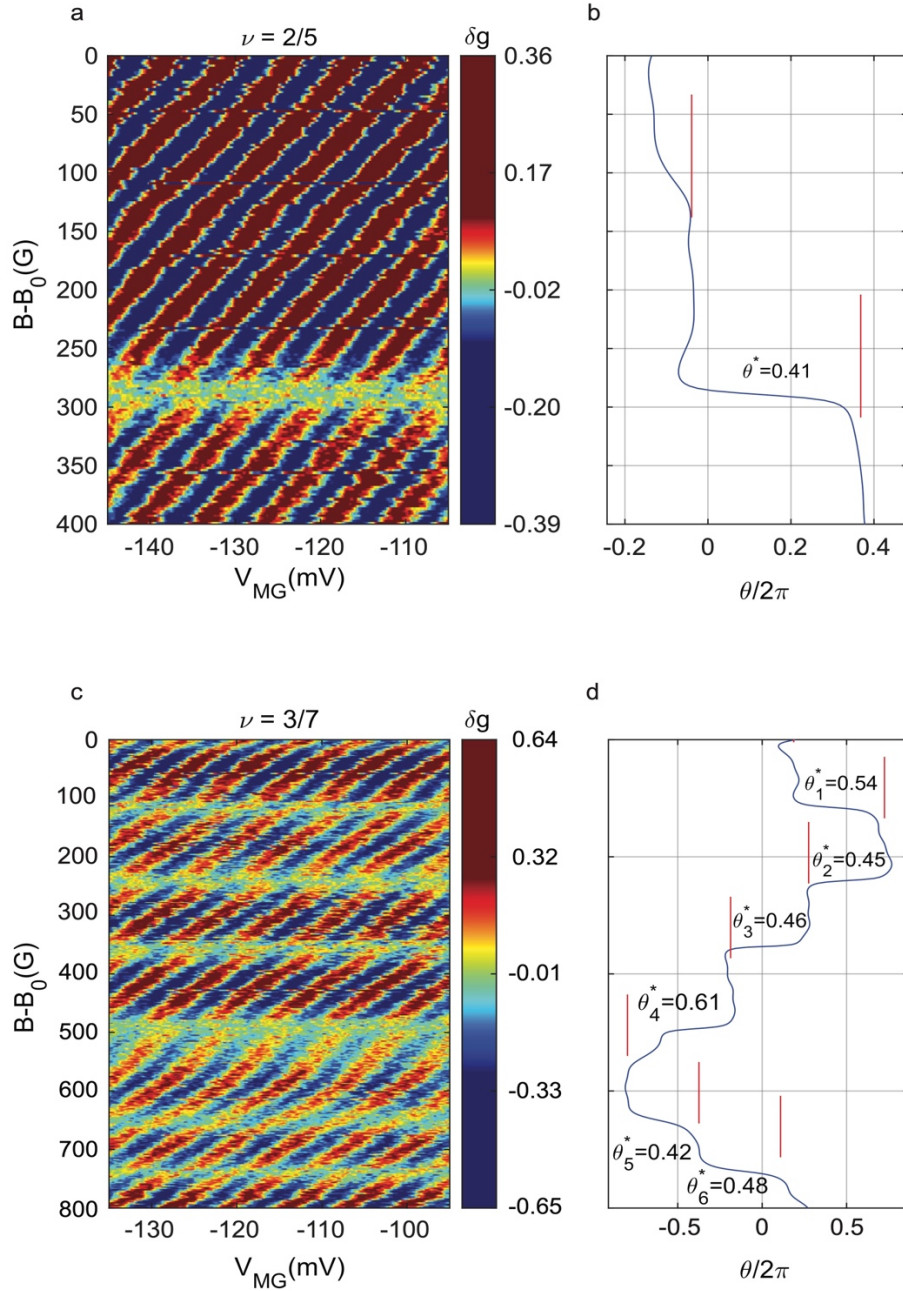


Figure S8: Aharonov Bohm pajamas with phase slips of the co-propagating outer edge mode in the bulk filling $\nu_t = 2/5$ and $3/7$. The conductance oscillation as a function of B and modulation gate voltage V_{MG} show Aharonov Bohm interference with clear phase jumps. For these measurements, the QPCs are biased to achieve 90% transmission of the bulk filling's outer 1/3 mode (a) (or middle 1/15 mode (c)) of 2/5 (or 3/7). The top gate voltage V_{TG} is tuned to -50mV to -90mV, far from complete depletion under the gate. The discrete phase jumps are similar to those observed for the corresponding innermost modes. Figures **b**, and **d** present the calculated phase slips with the Lock-In technique (see **Methods** and **S3**). The red lines indicate the regions of a constant phase.